# Efficient Techniques for Performance Enhancement in Intelligent Surface-enabled Wireless Networks

**Madi Makin,** MSc in Electrical and Computer Engineering

**Submitted in fulfillment of the requirements**
**for the degree of Master of Science**
**in Electrical and Computer Engineering**


**School of Engineering and Digital Sciences**
**Department of Electrical and Computer Engineering**
**Nazarbayev University**

53 Kabanbay Batyr Avenue,
Astana, Kazakhstan, 010000

**Supervisors:** Dr. Galymzhan Nauryzbayev, Dr. Aresh Dadlani

**April 2024**

# Declaration

I hereby declare that this manuscript, entitled "*Efficient Techniques for Performance Enhancement in Intelligent Surface-enabled Wireless Networks*", is the result of my own work except for quotations and citations which have been duly acknowledged.

I also declare that, to the best of my knowledge and belief, it has not been previously or concurrently submitted, in whole or in part, for any other degree or diploma at Nazarbayev University or any other national or international institution.

(signature of the author)

_ _ _ _ _ _ _ _ _ _ _ _ _ _ _ _

Name: Madi Makin

Date: 14 April 2024

# Abstract

Our study delves into the capabilities of Simultaneously Transmitting and Reflecting Reconfigurable Intelligent Surfaces (STAR-RIS) in boosting the performance of uplink-downlink (UL-DL) Non-Orthogonal Multiple Access (NOMA) networks. By segmenting STAR-RIS, we aim to improve NOMA users' channel gains, enhancing the efficiency of NOMA integration and obviating the necessity for UL power adjustments. We thoroughly examine our approach across two key optimization problems: feasible region and max-min rate (MMR), ensuring compliance with QoS demands for both UL-DL. Our method deploys the independent roles of STAR-RIS partitioning and Base Station (BS) transmission power to derive explicit formulas that reveal the effectiveness of optimal STAR-RIS portion in satisfying UL-QoS needs, while BS power management guarantees DL-QoS satisfaction. The robustness of our analytical conclusions is confirmed through simulation experiments, which underscore the substantial benefits STAR-RIS technology presents to NOMA networks under these varied operational frameworks.

# Acknowledgements

I would like to express my deepest appreciation to my supervisor Professor Galymzhan Nauryzbayev, who provided me with encouragement and patience throughout the work and who gave me the golden opportunity to do this wonderful project on the topic of wireless networks. I would also like to extend my deepest gratitude to Professor Aresh Dadlani for his great amount of assistance throughout the course of the research, who provided me with the necessary tools and insightful suggestions.

A special thanks to my family, friends, and loved ones. Their wise counsel and kind words led to the successful completion of this MSc Thesis.

# Table of Contents

# List of Abbreviations

| | |
|---|---|
| 2D | Two-Dimensional |
| 5G | Fifth Generation |
| 6G | Sixth Generation |
| AI | Artificial Intelligence |
| AN | Artificial Noise |
| ASC | Average Secrecy Capacity |
| AWGN | Additive White Gaussian Noise |
| BER | Bit Error Rate |
| CSI | Channel State Information |
| FD | Full-duplex |
| IoT | Internet of Things |
| MIMO | Multiple-Input Multiple-Output |
| NOMA | Non-Orthogonal Multiple Access |
| OMA | Orthogonal Multiple Access |
| OP | Outage Probability |
| PIN | Positive-Intrinsic-Negative |
| PLS | Physical Layer Security |
| QoS | Quality of Service |
| RF | Radio Frequency |
| RIS | Reconfigurable Intelligent Surface |
| SIC | Successive Interference Cancellation |
| SINR | Signal-to-Noise-plus-Interference Ratio |
| SOP | Secrecy Outage Probability |

# List of Figures

# List of Tables

# Chapter 1 – Introduction

## 1.1 Background

By the year 2030, it is forecasted that worldwide mobile data consumption will surge by more than 600-fold relative to the figures documented in 2010 [1]. This information underscores the significance of the progress and development of future communication technologies. Considering the advancements in fifth-generation (5G) communication, it's unlikely that they will entirely meet the escalating demand for wireless communication by 2030 [2]. The advancement of upcoming wireless networks, such as sixth-generation (6G) and beyond, comes with rigorous requirements and expectations to meet. Emerging technologies such as smart transportation systems, immersive virtual reality, and the industrial Internet of Things (IoT) will necessitate fast data speeds, extremely low delays, and massive connectivity, all achieved with a spectral and energy-efficient approach [3]. Hence, achieving high data rates with substantially lower energy consumption and implementation costs for 6G wireless networks remains essential.

Leveraging the notable advancements in programmable meta-materials, researchers are exploring an emerging technology aimed at enabling future wireless networks to accommodate challenging advancements. Reconfigurable Intelligent Surfaces (RISs) have recently attracted considerable interest due to their potential as a crucial technology aligning with the expected standards of future wireless networks. RIS is a metasurface that possesses metamaterial properties, giving an opportunity to control the transmission environment [4]. (dynamically shaping the properties of the transmitted signal between the transmitter and receiver). RIS can change the amplitude and/or the complex phase of the transmitted channel, reflecting and redirecting the signal to the destination, and enhancing the destination’s signal quality [5]. RIS is considered a potential candidate for future wireless technologies due to its

energy efficiency, allowing it to make a considerable boost in the performance of the end-user. Many researchers consider the deployment of RIS in different transmission scenarios with various configurations. For instance, in Figure 1 a potential implementation of RIS is illustrated. As can be seen, RIS is used in many setups, benefitting the information transfer in cellular networks, indoor communications, IoT networks, and even in the scale of a smart city. Compared to other technologies in the same area of research, RIS is cost-effective and does not require a high power supply as the conventional radio-frequency chains that are abundant in any active component.

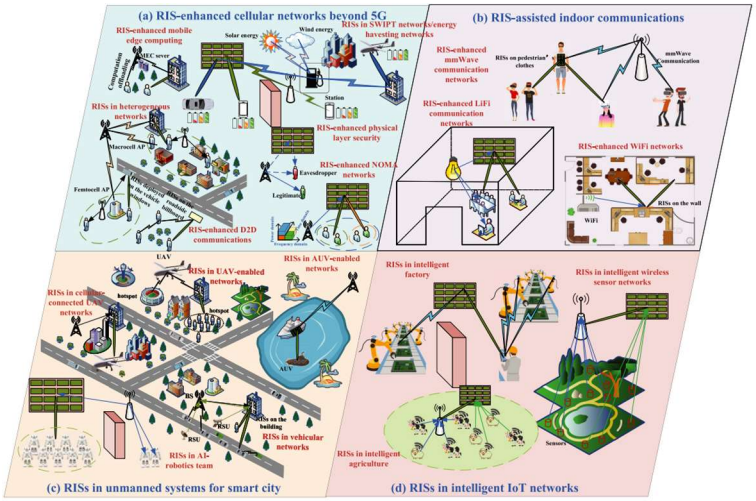


**Figure 1: Potential application of RIS in wireless networks [4].**

## 1.2 RIS Hardware Design

Compared to the existing transceiver technologies employed in wireless networks, the RIS concept offers unique attributes. Its key feature lies in enabling control over the environment by allowing the shaping and manipulation of the electromagnetic response of distributed objects within the network. Typically, a RIS structure serves as either a signal source or a wave collector with reconfigurable properties. This is particularly valuable in

scenarios where it functions as a passive reflector, aiming to enhance communication performance. RISs can be classified into active and passive types based on their power consumption and their corresponding design architectures will be discussed in proceedings.

### 1.2.1 Passive RIS design

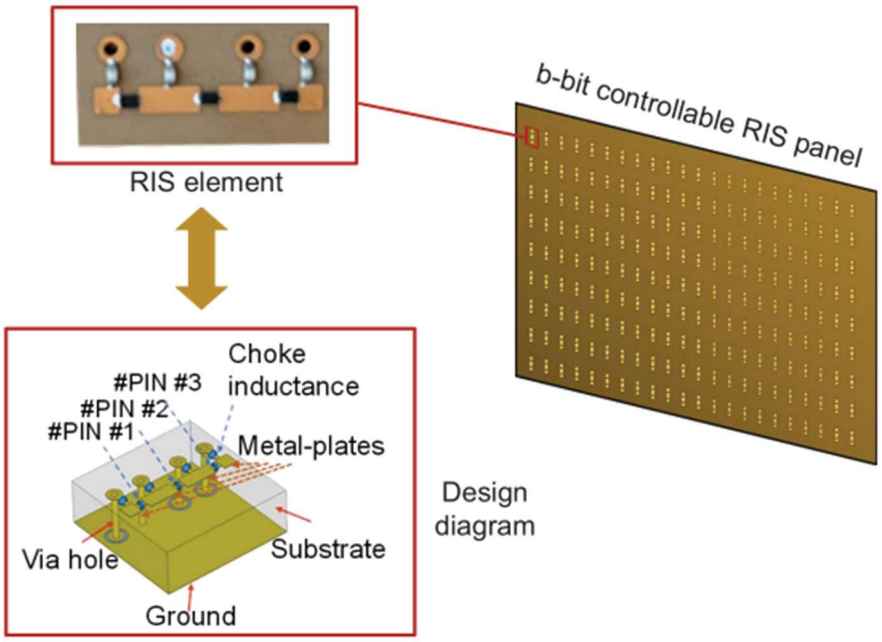


**Figure 2: Hardware design structure of passive RIS [6].**

Passive RIS's operational logic can be compared to a passive metal mirror or wave collector, having the ability to change the properties of the electromagnetic wave in a desired way [4]. Unlike active RIS, passive RIS is a more cost-efficient option that also does not require energy-intensive components integrated. The passive circuit design gives an opportunity to deploy energy harvesting modules to make the conventional RIS design even more energy-efficient [7]. The main advantage that makes the RIS concept appealing in a research community is not only its low-power consumption but also the elimination of radio frequency (RF) chains in design, which also results in removing the need for complex signal processing during deployment. Furthermore, passive RIS is full-duplex (FD) in nature and

can operate without any significant self-interference or noise cancellations [8]. The conventional hardware design of passive RIS is depicted in Figure 2. A 2D antenna array is made by a collection of radiative elements placed on a supporting structure. Each of these elements has its own electromagnetic characteristics with adjustable phase and amplitude, controlled by the element's polarizability. This polarizability is manipulated by the RIS controller through multiple positive-intrinsic-negative (PIN) diodes, which can be turned on or off as needed (ON or OFF states).

### 1.2.2 Active RIS design

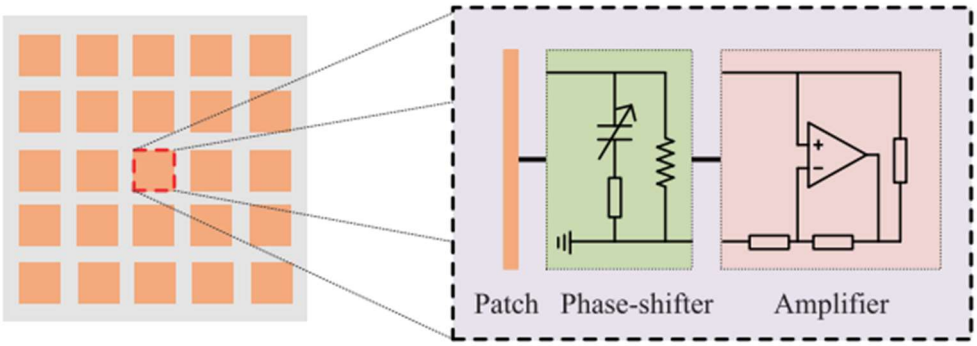


**Figure 3: Hardware design structure of active RIS [9].**

The term “active RIS” is used when the surface of RIS is embedded with power-hungry RF chains that are needed to perform any active signal processing procedures. Active RIS can be regarded as a natural evolutional step of conventional massive multiple-input multiple-output (MIMO) systems, as the concept of active RIS includes the integration of a two-dimensional (2D) array of software-controlled antenna elements. In [10], the authors investigated active RIS with decreased spacing between the elements while increasing the number of RIS pixels. By densely embedding multiple small active RIS elements alongside adaptable processing networks, it becomes feasible to establish a functional continuous

antenna aperture. With the assistance of the hologram principle, one can utilize RIS to both reflect and transmit the signal in the respected area of communication. One of the conventional design architectures of active RIS is depicted in Figure 3, where the active components of the array are used to amplify the reflected signal.

Even though there are many designs and integrations of active RISs in the literature, most research works are investigating the passive models of RISs in wireless communications. As the main merits of RIS are the cost and energy efficiency along with its passive nature, active RIS can be considered as a trade-off between energy efficiency and operational degree of freedom. Therefore, as with many other studies on RIS, this work investigates and implements the conventional passive RIS model that will be used in the proceeding system model design section.

### 1.3 Literature Review

RIS, as was described earlier is capable of shaping the amplitude and/or phase of the transmitted complex signal that allows canceling the interfering complex part of the channel and also tuning the signal by increasing its amplitude [7]. Owing to RIS's unique abilities, the attention from the researchers' community has increased, investigating RIS in the wireless networks research direction. As will be discussed in the proceeding subsection, RIS has many advantages that make it superior to other proposed technologies.

#### 1.3.1 RIS advantages

One of the advantages of RIS is defined in its physical characteristics. RIS is a flat passive metamaterial that can be easily deployed almost everywhere. As seen in Figure 1, RIS can be installed on buildings, walls, and windows. The size and weight of RIS make it available to be easily integrated with the already existing configurations, without redesigning and making any other bulky constructions to support the novel technology.

The spectrum efficiency criterion is described in the amount of data transmitted over the available spectrum or bandwidth [11]. RIS was reported to increase the spectrum efficiency of the system both by introducing novel transmission protocols and by being compatible with multiple users. An example related to novel protocols can be observed in [12], where the authors proposed a transmission scenario, where a single RIS can embed the signal messages of both users, transmitting them to the given base station (BS). On the contrary, the authors of [13] utilized the RIS to support multiple users to increase the spectral efficiency of the system.

### 1.3.2 Potential challenges

Along with the advantages that RIS introduces, there are many challenges with its implementation and design. Firstly, the performance of a RIS-aided system is usually analyzed with the assumption that RIS has the information on the global channel state information (CSI). In practical scenarios, RIS cannot possess the CSI of every channel link available [11]. CSI is the information on the known channel properties within the communication links. The information on signal propagation is required for RIS to work flawlessly, otherwise, no signal boost will be made, on the contrary, the signal quality will suffer and no reliable communication link will be achieved. Such a problem leads to a question – can one use RIS in a channel uncertainty (CSI uncertainty) medium? This question inspired many researchers in RIS-assisted system model investigation under limited or no CSI acquisition scenarios.

RIS, being an auxiliary node between the source and end-user has problems related to double path loss effects [11]. Since the signal is forced to travel a longer distance due to the obstacles in the direct communication link, it suffers from channel attenuations heavily. RIS is designed to compensate for such loss with constructive accumulation techniques, however,

a considerable number of reflective elements are required to achieve satisfactory signal gain. This will increase the size and cost of RIS, which is nonpreferred. There are several research directions to decrease the path loss effects by integrating multiple RISs, although such an approach increases the computational complexity.

### 1.3.2 Research Directions

The benefits RIS provides are utilized for performance enhancement in various system configurations. Further, the amalgamation of RIS with other technologies for various frameworks will be discussed.

#### 1.3.2.1 RIS and Multiple Access

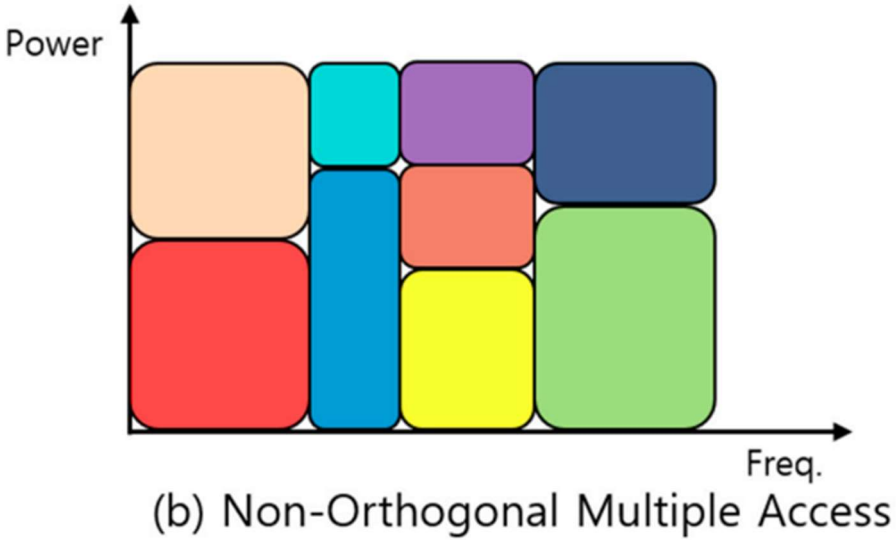


**Figure 4: Resource allocation in NOMA [14].**

Non-orthogonal multiple access (NOMA) is an innovative technique that allows multiple users to efficiently share a frequency spectrum. It enables each user to allocate bandwidth for transmitting signal messages, involving subsequent decoding and encoding steps as shown in Figure 4 [15]. This bandwidth allocation becomes crucial in scenarios with limited spectrum resources. While NOMA emerged as a promising option for adoption in 5G

networks, its complex protocols pose challenges that raise doubts about its suitability. The computational complexity of the NOMA protocol during successive interference cancellation (SIC) procedures exponentially grows with more users involved [16], which is impractical for massive connectivity.

By combining RIS and NOMA technologies, one can potentially boost system performance. RIS is tailored to amplify power gains, while NOMA improves spectrum efficiency and connectivity [17]. The authors of [18] studied RIS-assisted hybrid NOMA systems to enhance the energy and spectral efficiencies of conventional hybrid NOMA by pairing a near user with multiple far users and optimizing joint beamforming at the BS and RIS. Simulation results demonstrated that this proposed system achieves better sum-rate performance compared to conventional RIS-assisted NOMA and orthogonal multiple access systems, especially in scenarios with imperfect successive interference cancellation. In another work on NOMA [19], the authors designed the system to enhance wireless network performance by allocating fixed RIS units to each user, improving diversity order and signal quality. Analytical results demonstrated that the proposed system surpasses traditional NOMA in average sum-rate, outage probability (OP), and bit error rate (BER), particularly under imperfect SIC conditions. Research indicates that networks combining RIS and NOMA can leverage the strengths of both technologies, leading to substantial performance enhancements. In a relevant study [20], an RIS-empowered NOMA system model was examined. The findings showcased a noteworthy improvement in the network's outage performance and ergodic rate, highlighting the superiority of the RIS-NOMA fusion over traditional benchmark systems.

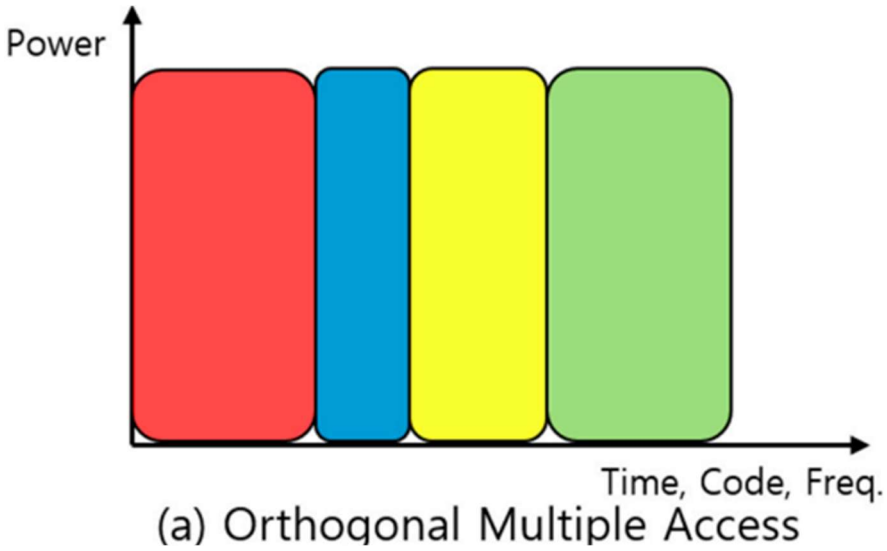


**Figure 5: Resource allocation in OMA [14].**

Another technology that, unlike NOMA, does not utilize the same communication resources during the transmission. Instead, the users are considered to be orthogonal, thus, the resource allocation ensures that no interference is caused within the network across the users [14]. Each user communicates within its own orthogonal channel as shown in Figure 5. The main idea of OMA is to enhance the network's reliability and quality by minimizing inter-user interferences. Compared to its orthogonal counterpart, NOMA systems are agreed to achieve better performances. This comparison, derived from a series of research works [17], [21]-[24], highlights the performance dynamics between NOMA and OMA, especially in the presence of RIS technology, which is pivotal for enhancing future wireless communication systems. In [21], the authors achieved better sum-rate and energy-efficiency performance for the RIS-aided system. It was shown that the sum-rate of the proposed NOMA network surpasses that of the OMA, attributing the advantage to NOMA's inherent multiplexing gain. In [23], the influence of RIS on user channels is noted as a significant factor in determining the superiority of NOMA over OMA. The benefits of RIS can make channel conditions between users more distinct, enhancing the NOMA gain. This adjustment of user channels

through RIS intervention makes NOMA potentially more advantageous than OMA, which typically benefits less from channel condition disparities. Finally, as was shown in a more focused study on vehicular communication [24], the performance of RIS-assisted NOMA is contrasted with OMA in vehicular communication networks. The work underscores that while RIS-assisted NOMA systems have been generally viewed as superior to OMA counterparts, this may not always hold true, especially in complex propagation environments like those in vehicular communications. This finding emphasizes the need to carefully consider the specific application scenario when choosing between NOMA and OMA in RIS-aided networks.

#### 1.3.2.2 RIS-assisted Physical Layer Security

Physical layer security (PLS) is a security measure that utilizes the physical settings of the available channel, ensuring the secrecy of the information transmitted [25]. Compared to conventional cryptography-based security, PLS can promote an additional layer of protection. RIS provided many interesting ideas in the direction of PLS. Since RIS is able to provide signal gain for the destined users, it was also found that RIS is capable of transmitting destructive electromagnetic waves. One can design the RIS to not only support the user and boost its signal quality but also destructively affect anyone who tries to eavesdrop on the data transmission. The authors of [26] investigated the PLS of the RIS-assisted system in the presence of a passive eavesdropper that tries to overhear the information transmitted. It was shown that RIS can improve security in the considered communication links. Such evaluation was illustrated with PLS metrics such as secrecy outage probability (SOP) and average secrecy capacity (ASC).

Another approach in RIS utilization for secrecy communication purposes is altering the transmission protocols as was shown in [27]. The authors proposed a phase-based adaptive modulation to ensure the security between the source and the user. First, the BS and the user agree on the modulation scheme to be used in the first transmission. Next, additional information is embedded within the first signal messages and with the help of RIS is reflected to the user. This supplementary information has the message on the modulation scenario that will be used in the next transmission. The security is achieved with the assistance of an endlessly changing modulation scheme, where the RIS plays a key role, embedding additional information inside the complex phase and boosting the signal's quality.

#### 1.3.2.3 STAR-RIS

A recent exploration has focused on a fresh concept called Simultaneously Transmitting and Reflecting (STAR)-RIS. STAR-RIS extends the capabilities of conventional RIS systems by integrating transmitting functionality. This enhancement enables an RIS to split the transmitted signal, facilitating the reflection and transmission of signal portions to destinations on both sides of the RIS. In a study outlined in [22], STAR-RIS was tailored for NOMA-enabled wireless networks, demonstrating its ability to offer an extended coverage range compared to conventional RIS-based systems. Another work, detailed in [28], introduced three modes for the STAR-RIS concept. The energy splitting mode divides the signal's energy into reflected and transmitted components—simultaneously reflecting and transmitting portions of the signal. The mode-switching mechanism categorizes STAR-RIS into subgroups, enabling one group to transmit the signal while another reflects it. Meanwhile, the time-switching mode schedules reflecting and transmitting operations across time periods, with STAR-RIS alternating between functioning as a transmitter and a reflector. The findings indicated that STAR-RIS outperformed conventional

RIS setups in terms of power consumption. The significance of the STAR-RIS concept lies in its ability to partition the RIS plane into smaller subgroups, a crucial aspect of a given report.

#### 1.3.2.4 Active RIS

The active RIS concept gives an opportunity for RIS to process other functions apart from passive reflection. With active components integrated into RIS, one can enable sophisticated signal processing for a rather wider range of applications. Conventionally, the active components are used to amplify the incident signal's amplitude and tune the quality of the signal not only by canceling the complex phase of the cascaded channels but also by utilizing amplification. Recently, the active elements were exploited to create artificial noise (AN) in the transmission environment [29]. RIS reflects and amplifies the signal, redirecting it to the end user while also transmitting pseudo-random noise, AN. The created noise ensures the communication link's secrecy, causing destructive interference to any unintended eavesdropper. The end user, possessing the information on the pseudo-random sequence of the AN can easily eliminate the noise during the decoding process. Thus, the AN concept can significantly enhance the PLS of the system, without causing any critical disruption in the medium.

#### 1.3.2.5 RIS partitioning

Most existing studies make use of the entire RIS plane for their designated purposes. Enabling multiple users often necessitates deploying multiple RISs, which proves to be economically impractical. In response, the concept of RIS partitioning emerged to address this challenge. This concept, introduced as a potential research direction in [30], involves virtually dividing the RIS plane into distinct portions, each designated for different applications.

Ultimately, the idealistic view towards such a concept includes the physical layer slicing, where each division is integrated with the relevant components or sensors. These groups are intended to perform a certain designed function and can be described as a local IoT network, where each branch is interconnected with the central controller. Figure 6 reveals more insights into this idea, where the multitask RIS design is illustrated. It can be seen that each of the slicings is integrated with the intended components that allow the cells to passively reflect, amplify, or even transmit the signal. Moreover, having an artificial intelligence (AI) module-empowered controller gives an opportunity to not only manipulate the physical properties of the incident signal but also perform complex signal processing functions. Eventually, such a concept will come at a high cost in current realities, nevertheless, it may become practical in the future.

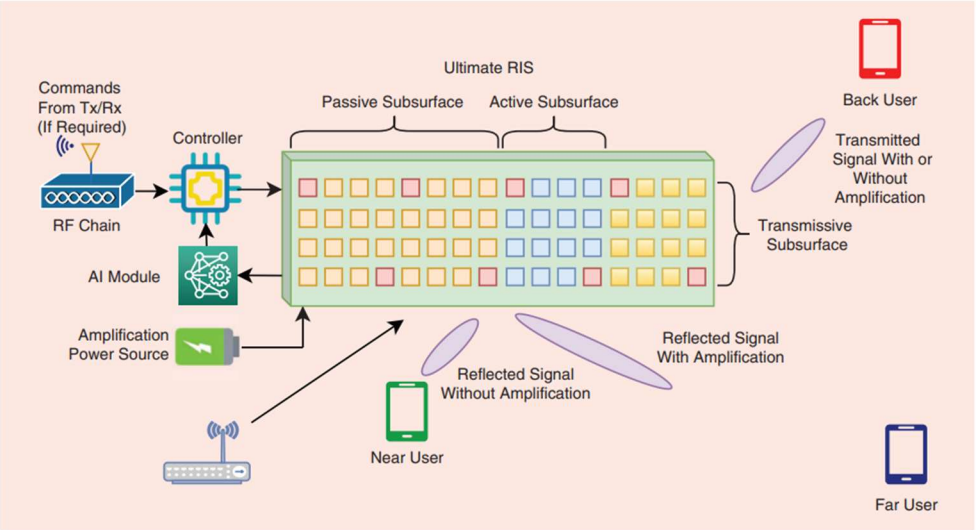


**Figure 6: Physical slicing of RIS [30].**

For now, RIS partitioning is used as a complementary technique that makes the combined technologies more practical. For instance, the authors of [31], proposed RIS partitioning for the NOMA network in the presence of SIC imperfections, evaluating the system's OP performance. It was shown that the conventional assumption of simultaneously

serving multiple NOMA users with no signal gain loss is impractical. RIS can redirect the maximum signal only in one direction, otherwise, the signal becomes scattered and the performance may become heavily reduced. One of the solutions to tackle this issue is to perform RIS partitioning to simultaneously redirect the signal received to the corresponding NOMA users. In such a manner, the NOMA users will get their signal messages to further proceed with the relevant NOMA signal decoding protocols.

### 1.4 Aims and Objectives

The partitioning concept is well implemented in STAR-RISs' practical operational protocols, nevertheless, the works being studied are mostly focused either on DL or UL. Inspired by the idea of RIS partitioning and NOMA, this work delves into STAR-RIS deployed NOMA network, investigating the bidirectional communication and assessing its performance by executing power control through optimization of STAR-RIS. Following the STAR-RISs coefficients' optimization, the system model will undergo analysis using optimization frameworks such as feasible region and max-min rate (MMR).

# Chapter 2 – Methodology

## 2.1 System model design

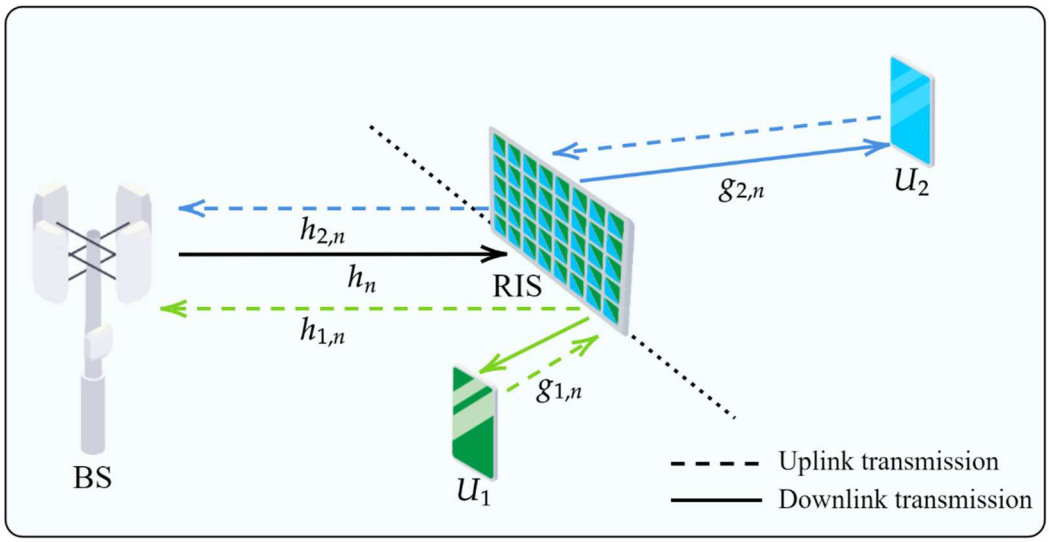


**Figure 7: STAR-RIS-aided NOMA network.**

The system model was designed to investigate the STAR-RIS-aided NOMA network as depicted in Figure 7. The figure showcases two signal transmission scenarios. The system model consists of two Users (*U*s) communicating to a BS with the aid of the STAR-RIS deployed with *N* number of passive elements. The users are positioned in designated areas by either transmitting or reflecting signals. Importantly, the proposed system model for MS can be expanded to cover scenarios where users are positioned in both transmission and reflection zones, without requiring modifications to the transmission protocol. Thus, to ensure adaptability, variables are assigned on an individual user basis instead of a transmission/reflection basis. The Nakagami-*m* fading model is used for the corresponding channel links [32]. The STAR-RIS is configured to assign a specific number of passive elements to each user, enhancing the quality of its transmission link. By leveraging STAR-RIS operational protocols, the system is designed to regulate power tailored to specific

conditions applied to the system, such as quality of service (QoS) requirements. Consequently, a $U_i$ receives a portion of its signal coherently aligned from its designated STAR-RIS segment. For practicability, the system is designed with the presence of imperfect SIC and CSI.

### 2.2 Signal Transmission

In this subsection, we outline the signal transmission for two-user NOMA networks assisted by STAR-RIS. It should be noted that serving many NOMA nodes comes with a large SIC complexity, as the number of nodes becomes large, increasing the computational complexity and, therefore, increasing the latency [16]. The signal transmission protocol for each scenario is defined with the corresponding receiving signal and signal-to-noise-plus-interference ratio (SINR) expressions.

#### 2.2.1 Downlink NOMA

In downlink NOMA, the signal is transmitted by BS through STAR-RIS to the $U_i$ can be expressed as

$$\breve{y}_i = \left[ \underbrace{\sum_{n=1}^{N_1} g_{i,n} h_n \psi_{i,n} e^{j\breve{\theta}_{i,n}}}_{aligned\ phase} + \underbrace{\sum_{n=1}^{N_2} g_{i,n} h_n \psi_{i,n} e^{j\breve{\theta}_{r,n}}}_{not\ aligned\ phase} \right] \sqrt{P_b} \left[ \sqrt{\beta_1} x_1 + \sqrt{\beta_2} x_2 \right] + n_i \qquad (1)$$

where $N_i = \lceil \alpha_i N \rceil$ and $N_r = \lceil \alpha_r N \rceil$, having $\alpha_i$ and $\alpha_r$ standing for STAR-RIS elements allocation coefficients, and $i, r \in \{1,2\}, i \neq r$ with $\alpha_i + \alpha_r \leq 1$; $N$ is the total number of STAR-RIS elements utilized; $P_b$ stands for the BS power transmitted, $\beta_1$ and $\beta_2$ are the corresponding power splits for DL-NOMA, $\beta_1 + \beta_2 \leq 1$; $g_{i,n}$ corresponds to the channel between $U_i$ and STAR-RIS's $n$th element; $h_n$ stands for the channel link between BS and STAR-RIS; $\psi_{i,n} = \left(d_{i,n} d_{n,b}\right)^{-\frac{\tau}{2}}$ with $d_{i,n}$ and $d_{n,b}$ standing for the distances of STAR-RIS-$U_i$ and STAR-RIS-BS links; $\tau$ corresponds to the path-loss coefficient; $n_i$ is the additive

white Gaussian noise (AWGN) with the corresponding variance $\sigma_i^2$. The phase-adjusting coefficients for the DL scenario are $\breve{\theta}_{i,n}$ and $\breve{\theta}_{r,n}$ and can be expressed as follows: $\breve{\theta}_{i,n} = -(\arg[g_{i,n}] + \arg[h_n])$. The existing form of the received signal poses analytical challenges due to its complexity. To tackle this problem, we suggest an approximate representation that improves tractability. Furthermore, prior research, such as [33], has shown that the influence of the non-aligned signal portion becomes insignificant with a sufficient number of reflective elements utilized. Therefore, in this study, we exclude the signal component stemming from the non-coherently aligned part of the RIS. As a result, the proposed signal representation in equation (1) can be formulated as

$$\breve{y}_i = \alpha_i \sum_{n=1}^{N} g_{i,n} h_n \psi_{i,n} e^{j\breve{\theta}_{r,n}} \sqrt{P_b}\left[\sqrt{\beta_1} x_1 + \sqrt{\beta_2} x_2\right] + n_i \qquad (2)$$

Nevertheless, the impact of the not-aligned part of the signal will be analyzed in the corresponding results section. Based on the practical CSI imperfection model outlined in [34] and [35], we presume that the CSI for the BS-STAR-RIS path is accurately known. However, the CSI knowledge for the STAR-RIS-$U_i$ the path is considered imperfect and adheres to the widely adopted imperfect CSI model, as considered in [36] and [37]. The corresponding channel link can be expressed as

$$g_{i,n} = \rho \bar{g}_{i,n} + \sqrt{1-\rho^2}\tilde{g}_{i,n}, \qquad (3)$$

where $\rho$ denotes the correlation parameter, $\bar{g}_{i,n}$ and $\tilde{g}_{i,n}$ are the estimated channel and CSI errors, respectively. The CSI error is modeled with zero mean and $\sigma_e^2$ variance complex Gaussian random variables. Following the NOMA protocol, we define $U_1$ as the strong user (having stronger channel conditions), and $U_2$ as the weak user. Next, the strong user, $U_1$ utilizes SIC to identify and remove the signal intended for $U_2$ from its received signal. Subsequently, $U_1$ decodes its own message. Conversely, $U_2$ deciphers its message while

considering the signal intended for $U_1$ as interference. Following this message transmission, we are able to formulate the corresponding signal-to-interference-to-noise ratios for each NOMA user as follows

$$\check{\gamma}_1(\boldsymbol{\alpha},\boldsymbol{\beta}) = \frac{\beta_1 P_b |\alpha_1 \check{A}_1|^2}{\epsilon\beta_2 P_b |\alpha_1 \check{B}_1|^2 + \beta_1 P_b |\alpha_1 \check{C}_1|^2 + \sigma_1^2}, \quad (4)$$

$$\check{\gamma}_1(\boldsymbol{\alpha},\boldsymbol{\beta}) = \frac{\beta_2 P_b |\alpha_2 \check{A}_2|^2}{\beta_1 P_b |\alpha_2 \check{B}_2|^2 + \beta_2 P_b |\alpha_2 \check{C}_2|^2 + \sigma_2^2}, \quad (5)$$

where $\check{A}_i = \sum_{n=1}^{N} \bar{\Psi}_{i,n} e^{j\check{\theta}_{i,n}}$, $\check{B}_i = \sum_{n=1}^{N} \Psi_{i,n} e^{j\check{\theta}_{i,n}}$, $\check{C}_i = \sum_{n=1}^{N} \tilde{\Psi}_{i,n} e^{j\check{\theta}_{i,n}}$, $\alpha = [\alpha_1, \alpha_2]$, $\beta = [\beta_1, \beta\_2]$, $\Psi_{\mathrm{i}} = g_{i,n} h_n \psi_{i,n}$, $\bar{\Psi}_{\mathrm{i}} = \rho g_{i,n} h_n \psi_{i,n}$, $\tilde{\Psi}_{\mathrm{i}} = \sqrt{1-\rho^2} g_{i,n} h_n \psi_{i,n}$; $\epsilon$ denotes the imperfect SIC coefficient.

### 2.2.1 Uplink NOMA

In the UL scenario, the power control is not enforced on the user's side. The power control is initialized with the help of STAR-RIS partitions by optimizing the portions needed for each NOMA user. In light of these points, the signals sent by the two users are mixed at the BS during the UL transmission in the following manner

$$\hat{y} = \left[\sqrt{P_1}\,\alpha_1 \sum_{n=1}^{N} \Upsilon_{1,\mathrm{n}}\, e^{j\hat{\theta}_{1,n}}\right] x_1 + \left[\sqrt{P_2}\,\alpha_2 \sum_{n=1}^{N} \Upsilon_{2,\mathrm{n}}\, e^{j\hat{\theta}_{2,n}}\right] x_2 + n_b\,, \quad (6)$$

where $\Upsilon_i = g_{i,n} h_{i,n} \psi_{i,n}$, $P_1$ and $P_2$ are the corresponding transmit powers of $U_1$ and $U_2$; $h_{i,k}$ is the channel link of STAR-RIS-BS delivering the signal of $U_i$, $n_b$ is AWGN with $\sigma_b^2$ variance. Similarly, as in DL, the phase-shifting coefficients $\hat{\theta}_{i,n}$ can be expressed as $\hat{\theta}_{i,n} = -(\arg[g_{i,n}] + \arg[h_{i,n}])$. Following (6), the corresponding SINRs can be written as

$$\hat{\gamma}_1 = \frac{P_1 |\alpha_1 \hat{D}_1|^2}{P_2 |\alpha_2 \hat{E}_2|^2 + P_1 |\alpha_1 \hat{F}_1| + \sigma_b^2}, \quad (7)$$

$$\hat{\gamma}_2 = \frac{P_2 |\alpha_2 \hat{D}_2|^2}{\epsilon P_1 |\alpha_1 \hat{E}_1|^2 + P_2 |\alpha_2 \hat{F}_2| + \sigma_b^2}, \quad (8)$$

where $\widehat{D}_i = \sum_{n=1}^{N} \overline{\Upsilon}_{\mathrm{i,n}}\, e^{j\widehat{\theta}_{i,n}}$, $\hat{E}_r = \sum_{n=1}^{N} \Upsilon_{\mathrm{i,n}}\, e^{j\widehat{\theta}_{i,n}}$, $\hat{F}_i = \sum_{n=1}^{N} \widetilde{\Upsilon}_{\mathrm{i,n}}\, e^{j\widehat{\theta}_{i,n}}$, $\overline{\Upsilon}_{i,n} = \rho \bar{g}_{i,n} h_{i,n} \psi_{i,n}$, $\widetilde{\Upsilon}_{i,n} = \sqrt{1-\rho^2}\, \bar{g}_{i,n} h_{i,n} \psi_{i,n}$. Compared to DL-SINR expressions defined in (4) and (5), the formulated UL-SINRs in (6) and (7) are solely affected by $\boldsymbol{\alpha}$, due to the lack of power control on the users' side. The protocol for UL-NOMA operates in a manner opposite to that of DL-NOMA. In the UL scenario, NOMA procedures are carried out by the BS, highlighting the importance of maintaining distinctions within the received superimposed signal. This differentiation is achieved by ensuring that users with equal transmit powers experience varying channel gains. Consequently, the user with a stronger signal exhibits greater signal strength and a more robust channel gain. In contrast to DL-NOMA, the decoding process in UL-NOMA involves treating messages from other users as interference to decode the message of the stronger user first. The weaker user's message is then decoded once the stronger user's message has been eliminated from the signal that was received.

### 2.3 Problem Formulation

This section begins by articulating the formal problem statements, followed by the development of the proposed solution approaches. Given the specified QoS requirements, we focus on obtaining the optimal STAR-RIS partitioning for two key optimization problems: the QoS feasible region, and the MMR. Each of these problems is elaborated upon in detail subsequently.

#### 2.3.1 Feasible Region

As a fundamental foundation for the subsequent optimization problems, our initial emphasis lies on the QoS feasible region, aiming to guarantee the fulfillment of QoS conditions for NOMA users in UL-DL transmissions. The feasibility region of the system is solved to aid in comprehending the viable regions of STAR-RIS portion allocations, thereby facilitating bidirectional traffic. In the end, this knowledge provides a foundation for

discussing the other optimization problems covered in the proceeding sections. We can formulate the system's feasibility as

$$\begin{aligned}
&\mathrm{P_f}: \quad \min_{\boldsymbol{\alpha},\boldsymbol{\beta}} \quad t \\
&\mathrm{C_f^1}: \quad \text{s.t.} \quad \check{\gamma}_{\mathrm{i}}(\boldsymbol{\alpha},\boldsymbol{\beta}) \geq \check{\gamma}_{\mathrm{th}}^{i}, i \in \{1,2\}, \\
&\mathrm{C_f^2}: \quad \hat{\gamma}_{\mathrm{i}}(\boldsymbol{\alpha}) \geq \check{\gamma}_{\mathrm{th}}^{i}, i \in \{1,2\}, \\
&\mathrm{C_f^3}: \quad \alpha_1 + \alpha_2 \leq 1, \\
&\mathrm{C_f^4}: \quad \beta_1 + \beta_2 \leq 1, \\
&\mathrm{C_f^5}: \quad \alpha_1 \in [0,1], \beta_{\mathrm{i}} \in [0,1], i \in \{1,2\},
\end{aligned} \tag{9}$$

where $\check{\gamma}_{th}^{i} = 2^{\mathrm{R_{th}}} - 1$ and $\hat{\gamma}_{th}^{i} = 2^{\mathrm{R_{th}}} - 1$ are the DL-UL QoS rate thresholds and $t$ is an arbitrary constant, $\mathrm{C_f^1}$ and $\mathrm{C_f^2}$ stand for the DL-UL QoS conditions, $\mathrm{C_f^3}$ and $\mathrm{C_f^4}$ are the total STAR-RIS elements and BS power allocation constraints; $\mathrm{C_f^5}$ is the domain of the parameters. To find optimal $\alpha_i$ range, the inequality in $\mathrm{C_f^2}$ is solved. Next, with the feasible range of $\boldsymbol{\alpha}$ the inequality in $\mathrm{C_f^1}$ solved to find the feasible $\boldsymbol{\beta}$ ranges. Therefore, the following lemmas outline the feasible range of STAR-RIS portions and BS power coefficients that satisfy the QoS conditions for both UL and DL scenarios.

*Lemma 1:* The range of feasible STAR-RIS elements that satisfy the given QoS constraints can be expressed as

$$\max_{j\in\{1,2\}}\{\hat{\alpha}_{i,l}^{j}\} \leq \alpha_i \leq \min_{j\in\{1,2\}}\{\hat{\alpha}_{i,v}^{j}\}, \tag{10}$$

where $\hat{\alpha}_{i,l}^{j}$ and $\hat{\alpha}_{i,v}^{j}$ are the corresponding lower-bound (LB) and upper-bound (UB) of the feasible region. The feasibility of the ranges in (10) must also adhere to the conditions specified in $\mathrm{C_f^3}$.

*Proof:* The LB and UB of the designated ranges determine the feasible region. For determining feasibility regions for NOMA users in DL-UL transmission, it is essential to

solve each objective function while considering the constraints outlined in $\mathrm{C}_{\mathrm{f}}^{3}$. Consequently, we substitute the separate SINRs from (7) and (8) into (9), resulting in the corresponding inequality for $U_1$

$$\frac{P_1\left[\alpha_1^1 D_1\right]^2}{P_2\left[\alpha_2^1 E_2\right]^2+P_1\left[\alpha_1^1 F_1\right]^2+\sigma_b^2} \geq \gamma_{\mathrm{th}}, \qquad (11)$$

where $\alpha_2^1 = 1 - \alpha_1^1$, $D_i, E_i$, and $F_i$ denote the real part of $\widehat{D}_i, E_i$, and $F_i$. Next, we structure the quadratic inequality

$$[\alpha_1^1]^2\, \bar{A}_1 + \alpha_1^1\, \bar{B}_1 + \bar{C}_1 \geq 0, \qquad (12)$$

where $\bar{A}_1 = P_1 D_1 - \gamma_{\mathrm{th}} P_1 F_1^2 - \gamma_{\mathrm{th}} P_2 E_2^2, \bar{B}_1 = 2\gamma_{\mathrm{th}} P_2 E_2^2, \bar{C}_1 = -\gamma_{\mathrm{th}}\sigma_b^2 - \gamma_{\mathrm{th}} P_2 E_2^2$. Applying the discriminant rule, the critical point of the inequality can be derived as

$$\alpha_{1,\{l,v\}}^1 = \frac{-\bar{B}_1 \pm \sqrt{\bar{B}_1^2 - 4\bar{A}_1\bar{C}_1}}{2\,\bar{A}_1}. \qquad (13)$$

Following the same steps, the roots for $U_2$ can be found as

$$\alpha_{1,\{l,v\}}^2 = \frac{-\bar{B}_2 \pm \sqrt{\bar{B}_2^2 - 4\bar{A}_2\bar{C}_2}}{2\,\bar{A}_2}, \qquad (14)$$

where $\bar{A}_2 = P_2 D_2 - \gamma_{\mathrm{th}} P_2 F_2^2 - \epsilon\gamma_{\mathrm{th}} P_1 E_1^2, \bar{B}_2 = -2P_2 D_2^2 + 2\gamma_{\mathrm{th}} P_2 F_2^2, \bar{C}_2 = -\gamma_{\mathrm{th}}\sigma_b^2 - \gamma_{\mathrm{th}} P_2 F_2^2 + P_2 D_2^2$.

*Lemma 2:* The range of feasible BS power splits that satisfy the given QoS constraints can be expressed as

$$\max_{j\in\{1,2\}}\{\check{\beta}_{i,l}^{j}\} \leq \alpha_i \leq \min_{j\in\{1,2\}}\{\check{\beta}_{i,v}^{j}\}, \qquad (15)$$

where $\check{\beta}_{i,l}^{j}$ and $\check{\beta}_{i,v}^{j}$ are the corresponding LB and UB of the feasible region. The feasibility of the ranges in (11) must also adhere to the conditions specified in $\mathrm{C}_{\mathrm{f}}^{4}$.

*Proof:* To find the feasible range of values of DL power splits we follow the same steps as in (11). First, rewriting the SINR for $U_1$

$$\frac{\beta_1^1 P_b[\alpha_1 A_1]^2}{\epsilon\beta_2^1 P_b[\alpha_1 B_1]^2+\beta_1^1 P_b[\alpha_1 C_1]^2+\sigma_1^2} \geq \gamma_{\text{th}}, \qquad (16)$$

where $\beta_2^1 = 1-\beta_1^1$, $A_i, B_i, C_i$ denote the real part of$\check{A}_i$, $\check{B}_i$, and $\check{C}_i$. Next, after using some algebraic manipulations we find the critical values for BS power splits

$$\beta_{1,\{l,v\}}^1 \geq \frac{\gamma_{\text{th}}\epsilon P_b[\alpha_1 B_1]^2+\gamma_{th}\sigma_1^2}{P_b[\alpha_1 A_1]^2-\gamma_{\text{th}}P_b[\alpha_1 C_1]^2+\gamma_{th}\epsilon P_b[\alpha_1 B_1]^2}. \qquad (17)$$

Similarly, the optimal DL power coefficients are found for $U_2$

$$\beta_{1,\{l,v\}}^2 \geq \frac{-P_b[\alpha_1 A_2]^2+\gamma_{\text{th}}P_b[\alpha_1 C_2]^2+\gamma_{\text{th}}\sigma_2^2}{-P_b[\alpha_1 A_2]^2+\gamma_{\text{th}}P_b[\alpha_2 C_2]^2-\gamma_{\text{th}}P_b[\alpha_2 B_2]^2}. \qquad (18)$$

### 2.3.1 Max-min Rate

In contrast to the predetermined QoS conditions in the feasible region optimization, the max-min problem seeks to maximize the minimum data rate attainable by both users in both the DL-UL transmissions. Consequently, the MMR problem for STAR-RIS partitions can be formulated as

$$\max_{\boldsymbol{\alpha}} \left( \min_{i\in\{1,2\}} \{\hat{\gamma}_i(\boldsymbol{\alpha}), \check{\gamma}_i(\boldsymbol{\alpha})\} \right) \text{ s.t. } \alpha_1+\alpha_2 \leq 1. \qquad (12)$$

Adhering to the conventional definition of MMR, the approach aims to maximize the minimum achievable transmission rate by maximizing the rate of the user with the worst channel gain, thereby boosting the system's overall performance. Consequently, this yields the optimal MMR that applies to all users in both DL-UL directions. It's important to note that the optimal MMR solution necessitates utilizing the entire STAR-RIS elements (i.e.,$\alpha_1 + \alpha_2 = 1$), thereby unifying the STAR-RIS partitioning parameters to a single variable

(i.e.,$\alpha_1 = \alpha, \alpha_2 = 1-\alpha, \beta_1 = \beta,$ and $\beta_2 = 1-\beta$). Defining the common rate threshold as an auxiliary variable $\mathrm{R_{th}}$, the problem in equation (12) can be expressed similarly as follows

$$\begin{aligned} \mathrm{P_m}: \quad & \max_{\alpha,\beta,\mathrm{R_{th}}} \quad \mathrm{R_{th}} \\ \mathrm{C_m^1}: \quad & \text{s.t.} \quad \check{\gamma}_{\mathrm{i}}(\alpha,\beta) \geq \check{\gamma}_{\mathrm{th}}^{i}, i \in \{1,2\}, \\ \mathrm{C_m^2}: \quad & \hat{\gamma}_{\mathrm{i}}(\alpha) \geq \check{\gamma}_{\mathrm{th}}^{i}, i \in \{1,2\}, \\ \mathrm{C_m^3}: \quad & \alpha \in [0,1], \beta \in [0,1], i \in \{1,2\}, \end{aligned} \tag{13}$$

where $\mathrm{C_m^1}$ and $\mathrm{C_m^2}$ denote the DL-UL QoS constraints, $\mathrm{C_m^3}$ is the domain of the parameters. The optimal MMR is determined by finding the solution to the system of equations defined by $\mathrm{C_m^1}$ and $\mathrm{C_m^2}$, i.e., $\check{\gamma}_1(\alpha,\beta) = \check{\gamma}_2(\alpha,\beta) = \hat{\gamma}_1(\alpha) = \hat{\gamma}_2(\alpha) = \mathrm{R_{th}}$. Employing a similar solution approach as outlined for the feasible region, first, the optimal STAR-RIS portions are defined for the UL scenario (the point where LB and UB are equal to each other), consequently, given obtained values of $\alpha$ the optimal $\beta$ is derived. Therefore, in the subsequent lemma the optimal portion, $\alpha^\star$, is calculated, which results in the UL-MMR for both users.

*Lemma 3:* The optimal STAR-RIS partitioning coefficient that achieves the UL-MMR can be expressed as

$$\alpha^\star = -\frac{b_p}{4a_p} + \frac{\pm_\mu \tilde{E}_2 \pm_\zeta \sqrt{-[3\,\tilde{A}_1 + 2\gamma_0 \pm_\mu \frac{2\,\tilde{B}_1}{\tilde{E}_2}]}}{2}, \tag{14}$$

where $\pm_\mu$ and $\pm_\zeta$ are independent. It is worth noting that only one root of optimal $\alpha^\star$ is resulting in MMR. During decision-making, three out of four roots are violating $\mathrm{C_m^3}$ in (13), leaving only one suitable solution.

*Proof:* To find optimal values that result in MMR we equate the corresponding SINRs from UL in (7) and (8) as

$$\frac{P_1[\alpha D_1]^2}{P_2[(1-\alpha)E_2]^2+P_1[\alpha F_1]^2+\sigma_b^2} = \frac{P_2[(1-\alpha)D_2]^2}{\epsilon P_1[\alpha E_1]^2+P_2[(1-\alpha)F_2]^2+\sigma_b^2}. \quad (15)$$

As discussed before, the MMR is defined in the UL scenario due to the lower power support in contrast to the DL case. Pushing the user with the weakest gain to its higher limits we obtain the following quartic equation also known as the fourth-degree polynomial

$$a_p[\alpha]^4 + b_p[\alpha]^3 + c_p[\alpha]^2 + d_p\alpha + e_p = 0, \quad (16)$$

where $a_p = P_2D_2^2P_1F_1^2 + P_2^2D_2E_2^2 - P_1D_1^2P_2F_2^2 - \epsilon P_1^2D_1^2E_1^2, b_p = -2P_2D_2^2P_1F_1^2 - 4P_2D_2^2 + 2P_1D_1^2P_2F_2^2, c_p = P_2D_2^2P_1F_1^2 + P_2D_2^2\sigma_b^2 + 6P_2^2D_2^2E_2^2 - P_1D_1^2P_2F_2^2 - P_1D_1^2\sigma_b^2, d_p = -2P_2D_2^2\sigma_b^2 - 4P_2^2D_2^2E_2^2, e_p = P_2D_2^2\sigma_b^2 + P_2^2D_2^2E_2^2$. Ferrari's method is used to solve this equation, as in [38]. Therefore, the final answer is shown in (14) and the rest notations are given: $\tilde{A}_1 = -\frac{3b_p^2}{8a_p^2} + \frac{c_p}{a_p}, \tilde{B}_1 = \frac{b_p^3}{8a_p^3} - \frac{b_pc_p}{2a_p^2} + \frac{d_p}{a_p}, \tilde{C}_1 = -\frac{3b_p^4}{2^8a_p^4} + \frac{c_pb_p^2}{2^4a_p^3} - \frac{b_pd_p}{4a_p^2} + \frac{e_p}{a_p}, \tilde{A}_2 = -\frac{\tilde{A}_1^2}{12} - \tilde{C}_1, \tilde{B}_2 = -\frac{\tilde{A}_1^3}{108} + \frac{\tilde{A}_1\tilde{C}_1}{3} - \frac{\tilde{B}_1^2}{8}, \tilde{C}_2 = -\frac{\tilde{B}_2}{2} + \sqrt{\frac{\tilde{B}_2^2}{4} + \frac{\tilde{A}_2^3}{27}}, \widetilde{D}_2 = \tilde{C}_2^{\frac{1}{3}}, \tilde{E}_2 = \sqrt{\tilde{A}_1 + 2y_0}.$

Finally, $y_0$ id defined as

$$y_0 = -\frac{5\tilde{A}_1}{6} + \begin{cases} -\tilde{B}_2^{\frac{1}{3}}, & \text{if } \widetilde{D}_2 = 0, \\ \widetilde{D}_2 - \frac{\tilde{A}_2}{3\widetilde{D}_2}, & \text{if } \widetilde{D}_2 \neq 0. \end{cases} \quad (17)$$

*Lemma 4*: Following the values obtained in (14), the optimal BS power splits that will result in optimal DL-MMR which is equal to UL-MMR can be found as

$$\beta^\star = \frac{-H_1 \pm \sqrt{H_1^2 - 4\,G_1I_1}}{2\,G_1}. \quad (18)$$

*Proof:* After finding optimal UL portions in (14), the values of $\alpha^\star$ are inserted into the corresponding DL SINRS equated. The expression can be written as

$$\frac{\beta P_b[\alpha^\star A_1]^2}{\epsilon(1-\beta)[\alpha^\star B_1]^2+\beta P_b[\alpha^\star C_1]^2+\sigma_1^2} = \frac{(1-\beta)P_b[(1-\alpha^\star)A_2]^2}{\beta P_b[(1-\alpha^\star)B_2]^2+(1-\beta)P_b[(1-\alpha^\star)C_2]^2+\sigma_2^2}. \quad (19)$$

Finally, we solve the quadratic equation after some algebraic manipulations and calculate the optimal BS power allocations as in (15) with the following notations defined: $\beta_2^\star = 1 - \beta^\star, G_1 = -P_b^2[(1-\alpha^\star)A_2]^2[\alpha^\star C_1]^2 + P_b^2\epsilon[\alpha^\star B_1]^2[(1-\alpha^\star)A_2]^2 + P_b^2[\alpha^\star A_1]^2[(1-\alpha^\star)C_2]^2 - P_b[(1-\alpha^\star)B_2]^2,\ H_1 = P_b^2[(1-\alpha^\star)A_2]^2\,[\alpha^\star C_1]^2 - P_b[(1-\alpha^\star)A_2]^2\sigma_1^2 - P_b^2[\alpha^\star A_1]^2[(1-\alpha^\star)C_2]^2 - P_b[\alpha^\star A_1]^2\sigma_2^2, I_1 = P_b^2\epsilon[\alpha^\star B_1]^2[(1-\alpha^\star)A_2]^2 + P_b[(1-\alpha^\star)A_2]^2\sigma_1^2$.

# Chapter 3 – Results & Discussions

In this chapter, the derived closed-form (CF) solutions are confirmed, evaluating the efficiency of the proposed bidirectional communication using different system parameters. The defined MMR and feasible region problems can also be transformed and addressed using the geometric programming (GP) method. In this approach, numerical solvers such as the GP toolbox provided by CVX were employed. Unless otherwise specified, the results are obtained using MATLAB with the default parameters outlined in Table I. To make a deeper analysis of the network, the results section is divided into two subsections: taking into account perfect CSI/SIC and considering imperfection in SIC and channel acquiring.

**Table 1: Table of parameters.**

| | |
|---|---|
| STAR-RIS elements | $N$ = [64, 96, 128, 256, 512] |
| BS-STAR-RIS path | $d_{n,b} = 150$ m |
| STAR-RIS-$U_1$ path | $d_{1,n} = 59$ m |
| STAR-RIS-$U_2$ path | $d_{2,n} = 61$ m |
| Noise power | $\sigma_i^2 = \sigma_b^2 = -60$ dBm |
| BS transmit power | $P_b = 30$ dBm |
| $U_i$ transmit power | $P_i = 10$ dBm |
| Pass loss | $\tau = 2.2$ |
| $m$ shaping parameter | $m = [1,2,3]$ |
| Rate threshold constraint | $\mathrm{R_{th}} = 2$ bits/s/Hz |
| Correlation coefficient | $\rho = 0.9$ |
| Imperfect SIC coefficient | $\epsilon = [0.1,0.2,0.3]$ |

### 3.1 Perfect SIC/CSI

In this section, we explore the scenario where perfect conditions for CSI and SIC are assumed. The findings illustrate the influence of system parameters: Nakagami-*m* parameter, rate threshold value, distances between users, the number of STAR-RIS elements, and inclusion of the not-aligned part of the signal on the system's performance.

#### 3.1.1 Feasible Region

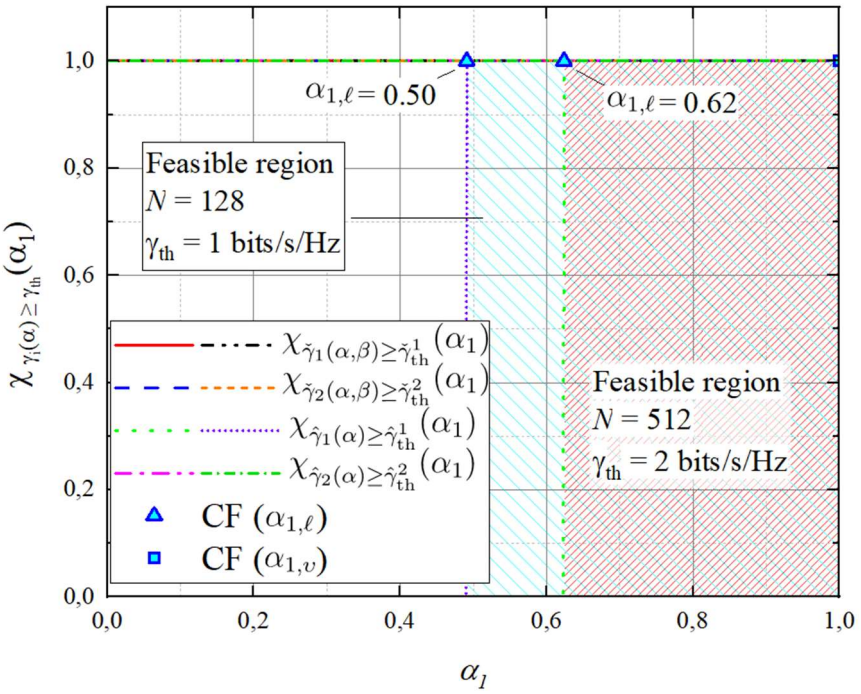


**Figure 8: Derived feasibility regions.**

Simulation results are provided in this subsection to confirm the analytically obtained solutions for the feasible region described in Lemma 1. To achieve this, we introduce the subsequent indicator function to evaluate the system's feasibility: $\chi_{\mathrm{A}}(x)=1,$ if $x\in A,$ and $\chi_{\mathrm{A}}(x)=0,$ otherwise.

Figure 8 depicts the feasible region of the system under various parameter configurations. The y-axis in the plot represents the fulfillment of the conditions $C_f^1$ and $C_f^2$ as defined in (9) ($\chi_{\hat{\gamma}_i \geq \gamma_{th}^i}(\alpha_1)\ and\ \chi_{\check{\gamma}_i \geq \gamma_{th}^i}$). The system's feasibility occurs when all users in the network exceed the specified QoS conditions. In this work, these conditions are met when the SINR values of NOMA users surpass the rate threshold value. Following (20), if the conditions are met, a binary one is assigned. Otherwise, if the rate threshold value is not reached, indicating non-feasibility, a zero value is assigned. In this figure, two system configurations were set: $N = 128$ and $R_{th} = 1$ bits/s/Hz, and the other with $N = 512$ and $R_{th}$= 2 bits/s/Hz. In the latter scenario, the system is feasible when the value of $\alpha_1$ lies between 0.62 and 1. Conversely, in the preceding situation, the feasible region expands, spanning from 0.5 to 1, owing to reduced QoS requirements. The simulated results closely correspond with the analytical ones, defined by the UB and LB. These bounds outline the range of values required to meet the QoS constraints. In this proposed system, the feasibility region is delineated by the range of $\alpha_1$ values ensuring that all users' rates exceed the defined rate thresholds. As the QoS threshold rises, this area decreases in width until the LB and UB converge, indicating the optimal STAR-RIS partitioning coefficient for achieving the MMR for DL-UL transmissions.

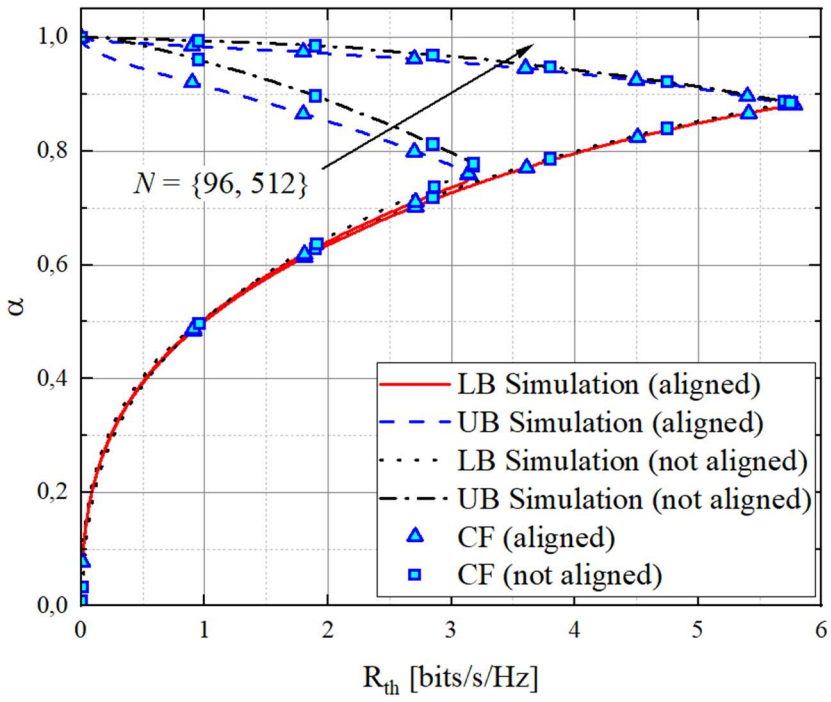


**Figure 9: Feasible regions for different $R_{th}$.**

In Figure 9, we can see a visual depiction of the feasible region, which shows how different values of the rate threshold and $\alpha_1$ affect the system's feasibility for various $N$ and configurations of the STAR-RIS. It is shown that the analytical results proposed for the UB-LB match well with the actual performance observed in simulations, confirming the accuracy of our calculations. Moreover, when comparing scenarios with aligned and non-aligned phases, we find that the performance difference is minimal, especially when there are many STAR-RIS elements involved. This supports the assumption we made in our analysis.

### 3.1.2 Max-min Rate

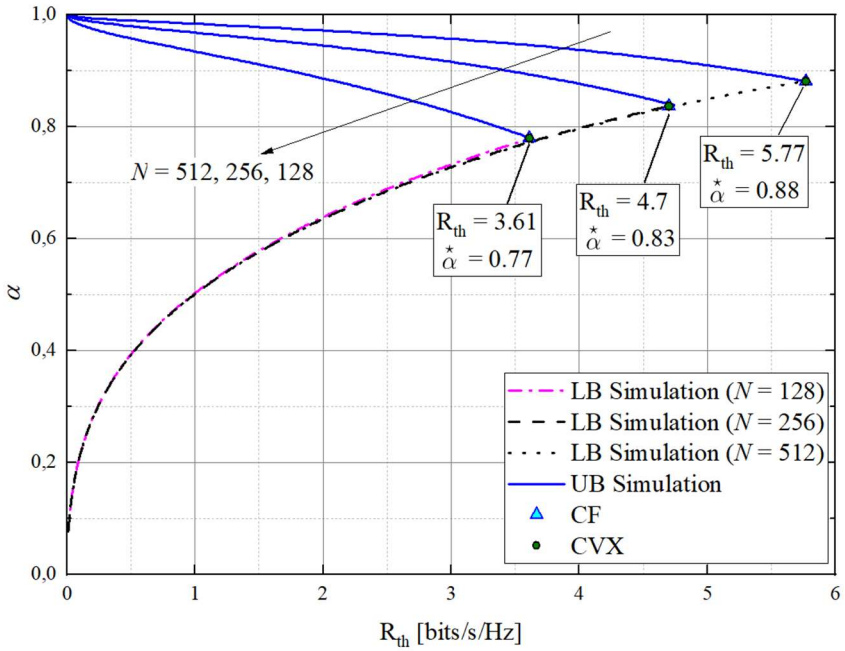


**Figure 10: MMR for various N and $R_{th}$.**

In Figure 10, we can see the performance of UL-MMR. The CF results for the optimal STAR-RIS portion, as derived in Lemma 3, closely match the numerical solutions obtained with CVX, providing strong evidence for the accuracy of our analytical derivations. We observe that the MMR enhances as the size of allocated STAR-RIS portions grows. For example, when the overall number of passive elements rises from 128 to 512, we achieve a remarkable 47% boost in MMR. Correspondingly, the optimal RIS portion, $\alpha^{\star}$, rises from 0.77 to 0.88. It's noteworthy that the enhancement in performance with more elements predominantly affects the UB curves. This is due to the SINR of $U_1$, which is influenced by interference from $U_2$ during UL transmission. Consequently, the gain of $U_1$ remains similar regardless of the STAR-RIS size deployed.

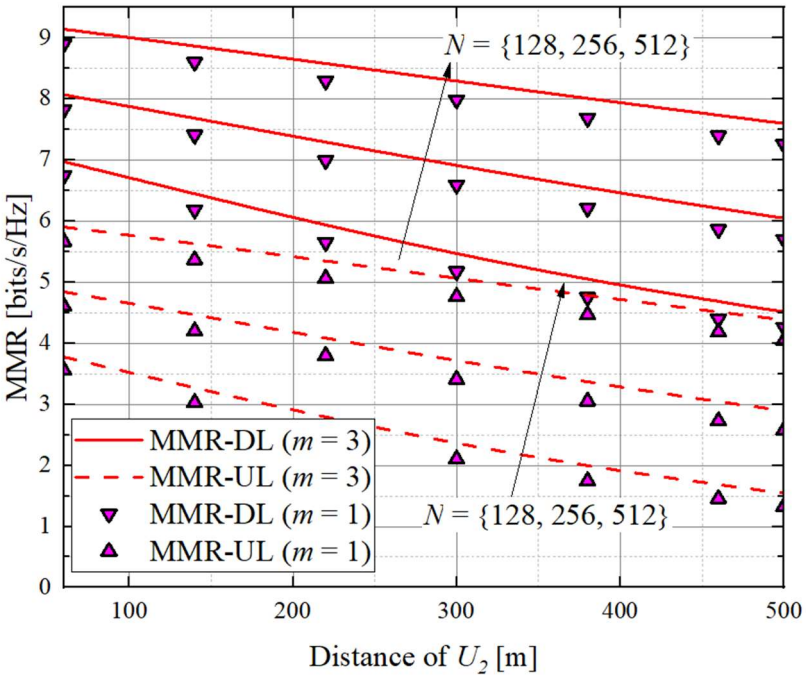


**Figure 11: MMR vs. $U_2$ distance.**

In Figure 11, we delve into the MMR outcomes for NOMA users, considering diverse simulation parameters by varying $U_2$ distances and the number of passive elements utilized. To achieve these results, we conduct iterative optimizations given $U_2$ distance. The graph illustrates that as $U_2$ moves farther away from the STAR-RIS, the system's MMR performance declines due to increased signal loss. Moreover, it highlights that increasing the number of STAR-RIS elements leads to a consistent enhancement in system performance. When $U_2$ is set 300 meters away and the $m$ parameter is set to $m = 3$, the MMR for DL transmission increases from 6.7 to 7.8 bits/s/Hz as the overall size of STAR-RIS enhances from 128 to 256. Moreover, this improvement further extends to 9 bits/s/Hz when $N$ equals 512. The graph also demonstrates the notable impact of the $m$ on the system's MMR. With $m = 1$, the channel follows the Rayleigh fading model, resulting in decreased MMR performance. This fading model better suits communication with no line of sight. Conversely, elevating the value of $m$ enhances MMR as the $m$ parameter also denotes the number of

multi-path components in the channel. A higher $m$ value signifies more multi-paths, offering increased diversity.

### 3.2 Imperfect SIC/CSI

In this subsection, the impact of channel and SIC imperfections are analyzed and discussed.

#### 3.2.1 Feasible Region

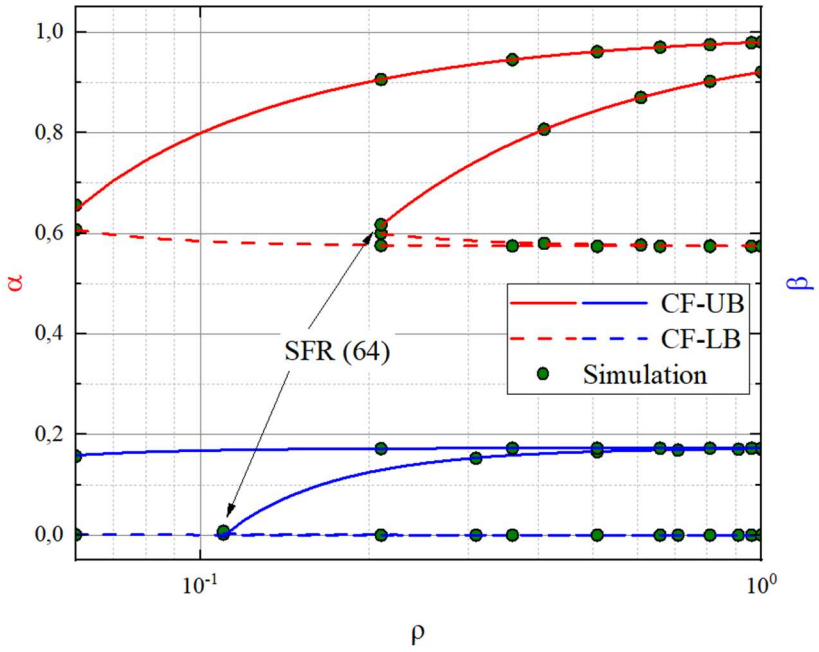


**Figure 12: Impact of ρ on feasible regions.**

In Figure 12, we can see how the LB and UB of the optimal ranges for $\alpha$ and $\beta$ vary, relative to the imperfect CSI coefficient. It's important to note that in this specific scenario, the imperfections in SIC are disregarded. The feasible region is defined as the interval spanning from the LB to the UB, starting at the beginning of the feasible region (SFR) and ending at the end of the feasible region (EFR) for each parameter. The results show a close match between the proposed analytical bounds outlined in Appendices A and B and the simulated outcomes, which validates the accuracy of our derivations. For $N = 256$, the

problem remains feasible across the entire range of $\rho$, regardless of the allocation of transmit power and the number of STAR-RIS elements. However, when reducing the total number of passive elements, the feasible region shrinks, making the problem feasible for α only when ρ exceeds 0.21. It's noteworthy that the feasible region for the optimal $\beta$ is more resilient to CSI imperfections compared to that of $\alpha$, especially evident when $N = 64$.

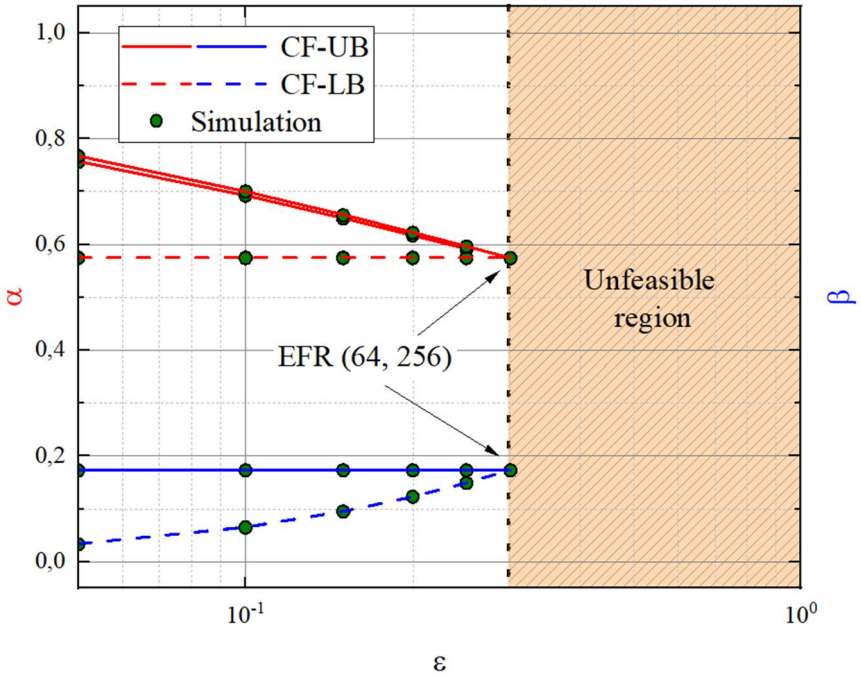


**Figure 13: Impact of ϵ on feasible regions.**

In Figure 13, a similar methodology was utilized, with imperfect SIC displayed on the x-axis. Perfect CSI conditions were maintained to specifically analyze the impact of $\epsilon$. The results highlight that imperfect SIC detrimentally impacts the system's feasibility, regardless of the number of passive elements deployed. Once ϵ exceeds 0.25, the system reaches the EFR. Unlike CSI imperfections, imperfections in SIC have a more pronounced effect due to the heightened interference they introduce. Remarkably, almost identical feasible regions were observed for both $N = 256$ and $N = 64$. This similarity arises because $\epsilon$ affects only one

of the users in the NOMA system, and the degree of imperfection increases proportionally with the allocation of reflective elements.

### 3.2.2 Max-min Rate

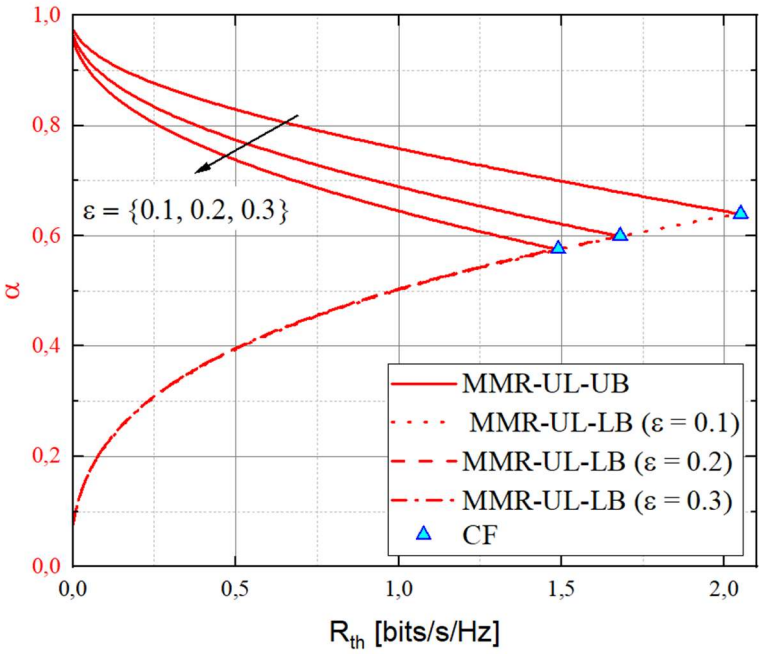


**Figure 14: UL-MMR for various ϵ values.**

Figure 14 depicts the MMR-UL transmission scenario for N = 128, where the CF solutions for the optimal STAR-RIS portion are derived as presented in Lemma 3, and closely align with the simulated results, validating the accuracy of the analytical derivations. As $\epsilon$ increases, there is a noticeable decrease in the achievable MMR. The users reach the maximum rate threshold at 2.05 bits/s/Hz, while the minimum threshold, influenced by SIC imperfections, stands at 1.49 bits/s/Hz. It's worth noting that changes in ϵ only impact the UB curves, as interference is only present on the weaker user's side.

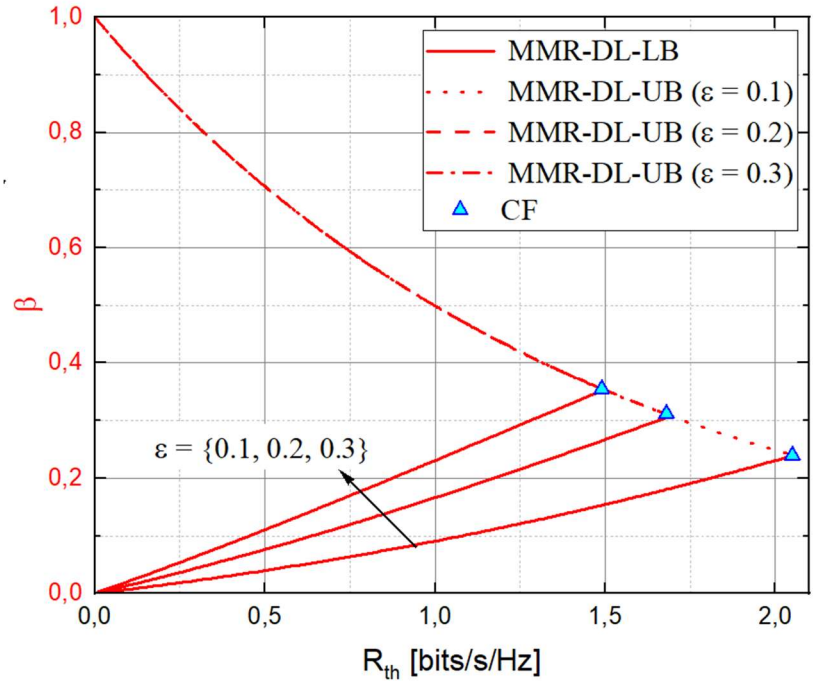


**Figure 15: DL-MMR for various ϵ values.**

Figure 15 demonstrates the relationship between the MMR and the corresponding BS power split coefficients for $N = 128$. Similarly, the increasing impact of SIC imperfections affects the achieved MMR. Interestingly, alterations in $\epsilon$ result in changes in the LB curves, contrasting with the UL scenario depicted in Figure 8. This difference highlights the distinction between UL and DL transmissions: in UL, a weak user undergoes SIC procedures, whereas in DL, a strong user employs SIC to decode its own signal message. The transition from $\epsilon = 0.1$ to $\epsilon = 0.3$ reduces the MMR by 28%, from 2.05 bits per second per hertz to 1.49 bits per second per hertz.

# Chapter 4 – Conclusion

The thesis investigated the influence of STAR-RIS on DL-UL NOMA networks. We used STAR-RIS mode-switching protocol that partitions RISs to optimize NOMA channel gains, leading to improved NOMA gain and eliminating the need for power control in the UL scenario. The proposed technique is comprehensively analyzed under key optimization problems, feasible region and MMR. The derived CF solutions illustrated how optimal allocation of STAR-RIS elements can meet UL-QoS requirements, while optimal BS power splits ensure DL-QoS satisfaction. To enhance the practicality of our proposed schemes, we considered imperfections in SIC and CSI. We optimized the corresponding parameters of the STAR-RIS to improve performance, and our findings showed that imperfect SIC had a more significant impact on the system's performance compared to imperfect CSI. Simulations validate our findings, demonstrating the significant benefits that STAR-RIS can offer in NOMA networks in UL-DL scenarios. Future work can concentrate on the implementation of the user pairing and user clustering concepts. This will enable accommodating a substantial number of NOMA users across numerous STAR-RISs dispersed throughout the communication area. Additionally, an AI approach can be assessed to reveal more insights into the system's performance and complexity.

# Bibliography


[1] Akhtar, M.W., Hassan, S.A., Ghaffar, R. *et al*., "The shift to 6G communications: vision and requirements," *Human-centric Computing and Information Sciences*, vol. 53, no. 10, 2020, https://doi.org/10.1186/s13673-020-00258-2.

[2] S. Basharat, S. A. Hassan, H. Pervaiz, A. Mahmood, Z. Ding and M. Gidlund, "Reconfigurable Intelligent Surfaces: Potentials, Applications, and Challenges for 6G Wireless Networks," *IEEE Wireless Communications*, vol. 28, no. 6, pp. 184-191, December 2021, doi: 10.1109/MWC.011.2100016.

[3] W. Saad, M. Bennis and M. Chen, "A Vision of 6G Wireless Systems: Applications, Trends, Technologies, and Open Research Problems," *IEEE Network*, vol. 34, no. 3, pp. 134-142, May/June 2020, doi: 10.1109/MNET.001.1900287.

[4] Y. Liu *et al*., "Reconfigurable Intelligent Surfaces: Principles and Opportunities," *IEEE Communications Surveys & Tutorials*, vol. 23, no. 3, pp. 1546-1577, 2021, doi: 10.1109/COMST.2021.3077737.

[5] G. C. Alexandropoulos, N. Shlezinger and P. del Hougne, "Reconfigurable Intelligent Surfaces for Rich Scattering Wireless Communications: Recent Experiments, Challenges, and Opportunities," *IEEE Communications Magazine*, vol. 59, no. 6, pp. 28-34, June 2021, doi: 10.1109/MCOM.001.2001117..

[6] B. Di, H. Zhang, L. Song, Y. Li, Z. Han and H. V. Poor, "Hybrid Beamforming for Reconfigurable Intelligent Surface based Multi-User Communications: Achievable Rates With Limited Discrete Phase Shifts," *IEEE Journal on Selected Areas in Communications*, vol. 38, no. 8, pp. 1809-1822, Aug. 2020, doi: 10.1109/JSAC.2020.3000813.

[7] E. Basar, M. Di Renzo, J. De Rosny, M. Debbah, M. -S. Alouini and R. Zhang, "Wireless Communications Through Reconfigurable Intelligent Surfaces," *IEEE Access*, vol. 7, pp. 116753-116773, 2019, doi: 10.1109/ACCESS.2019.2935192

[8] M. Jian *et al.*, "Reconfigurable intelligent surfaces for wireless communications: Overview of hardware designs, channel models, and estimation techniques," *Intelligent and Converged Networks*, vol. 3, no. 1, pp. 1-32, March 2022, doi: 10.23919/ICN.2022.0005.

[9] Q. Zhu, M. Li, R. Liu, Y. Liu and Q. Liu, "Joint Beamforming Designs for Active Reconfigurable Intelligent Surface: A Sub-Connected Array Architecture," *IEEE Transactions on Communications*, vol. 70, no. 11, pp. 7628-7643, Nov. 2022, doi: 10.1109/TCOMM.2022.3212749.

[10] S. Hu, F. Rusek and O. Edfors, "Beyond Massive MIMO: The Potential of Positioning With Large Intelligent Surfaces," *IEEE Transactions on Signal Processing*, vol. 66, no. 7, pp. 1761-1774, 1 April1, 2018, doi: 10.1109/TSP.2018.2795547.

[11] X. Yuan, Y. -J. A. Zhang, Y. Shi, W. Yan and H. Liu, "Reconfigurable-Intelligent-Surface Empowered Wireless Communications: Challenges and Opportunities," *IEEE Wireless Communications*, vol. 28, no. 2, pp. 136-143, April 2021, doi: 10.1109/MWC.001.2000256.

[12] H. Q. Ngo, E. G. Larsson and T. L. Marzetta, "Energy and Spectral Efficiency of Very Large Multiuser MIMO Systems," *IEEE Transactions on Communications*, vol. 61, no. 4, pp. 1436-1449, April 2013, doi: 10.1109/TCOMM.2013.020413.110848.

[13] M. Jung, W. Saad and G. Kong, "Performance Analysis of Active Large Intelligent Surfaces (LISs): Uplink Spectral Efficiency and Pilot Training," *IEEE Transactions on Communications*, vol. 69, no. 5, pp. 3379-3394, May 2021, doi: 10.1109/TCOMM.2021.3056532.

[14] J, Cheon, H-S. Cho, "Power Allocation Scheme for Non-Orthogonal Multiple Access in Underwater Acoustic Communications," *Sensors*, vol. 17, no. 11, pp. 2465, 2017. https://doi.org/10.3390/s17112465.

[15] Y. Saito, Y. Kishiyama, A. Benjebbour, T. Nakamura, A. Li and K. Higuchi, "Non-Orthogonal Multiple Access (NOMA) for Cellular Future Radio Access," *2013 IEEE 77th Vehicular Technology Conference (VTC Spring)*, Dresden, Germany, 2013, pp. 1-5, doi: 10.1109/VTCSpring.2013.6692652.

[16] Z. Ding, M. Peng and H. V. Poor, "Cooperative Non-Orthogonal Multiple Access in 5G Systems," *IEEE Communications Letters*, vol. 19, no. 8, pp. 1462-1465, Aug. 2015, doi: 10.1109/LCOMM.2015.2441064.

[17] Y. Cheng, K. H. Li, Y. Liu, K. C. Teh and H. Vincent Poor, "Downlink and Uplink Intelligent Reflecting Surface Aided Networks: NOMA and OMA," *IEEE Transactions on Wireless Communications*, vol. 20, no. 6, pp. 3988-4000, June 2021, doi: 10.1109/TWC.2021.3054841.

[18] M. H. Kumar, S. Sharma, K. Deka and M. Thottappan, "Reconfigurable Intelligent Surfaces Assisted Hybrid NOMA System," *IEEE Communications Letters*, vol. 27, no. 1, pp. 357-361, Jan. 2023, doi: 10.1109/LCOMM.2022.3211292.

[19] A. Chauhan, S. Ghosh and A. Jaiswal, "RIS Partition-Assisted Non-Orthogonal Multiple Access (NOMA) and Quadrature-NOMA With Imperfect SIC," *IEEE Transactions on Wireless Communications*, vol. 22, no. 7, pp. 4371-4386, July 2023, doi: 10.1109/TWC.2022.3224645.

[20] T. Hou, Y. Liu, Z. Song, X. Sun, Y. Chen and L. Hanzo, "Reconfigurable Intelligent Surface Aided NOMA Networks," *IEEE Journal on Selected Areas in Communications*, vol. 38, no. 11, pp. 2575-2588, Nov. 2020, doi: 10.1109/JSAC.2020.3007039.

[21] C. Wu, X. Mu, Y. Liu, X. Gu and X. Wang, "Resource Allocation in STAR-RIS-Aided Networks: OMA and NOMA," *IEEE Transactions on Wireless Communications*, vol. 21, no. 9, pp. 7653-7667, Sept. 2022, doi: 10.1109/TWC.2022.3160151.

[22] C. Wu, Y. Liu, X. Mu, X. Gu and O. A. Dobre, "Coverage Characterization of STAR-RIS Networks: NOMA and OMA," *IEEE Communications Letters*, vol. 25, no. 9, pp. 3036-3040, Sept. 2021, doi: 10.1109/LCOMM.2021.3091807.

[23] B. Zheng, Q. Wu and R. Zhang, "Intelligent Reflecting Surface-Assisted Multiple Access With User Pairing: NOMA or OMA?," *IEEE Communications Letters*, vol. 24, no. 4, pp. 753-757, April 2020, doi: 10.1109/LCOMM.2020.2969870.

[24] A. A. Salem, M. Rihan, L. Huang and A. Benaya, “Intelligent Reflecting Surface Assisted Hybrid Access Vehicular Communication: NOMA or OMA Contributes the Most?,” *IEEE Internet of Things Journal*, vol. 9, no. 19, pp. 18854-18866, 1 Oct.1, 2022, doi: 10.1109/JIOT.2022.3162787.

[25] Y. -S. Shiu, S. Y. Chang, H. -C. Wu, S. C. . -H. Huang and H. -H. Chen, “Physical layer security in wireless networks: a tutorial,” *IEEE Wireless Communications*, vol. 18, no. 2, pp. 66-74, April 2011.

[26] A. U. Makarfi *et al*., “Reconfigurable intelligent surfaces-enabled vehicular networks: A physical layer security perspective,” 2020. [Online]. Available: arxiv:2004.11288.

[27] M. Makin, S. Arzykulov, A. Celik, A. M. Eltawil and G. Nauryzbayev, “Enhancing Physical Layer Security in Large Intelligent Surface-aided Cooperative Networks,” *2022 IEEE 95th Vehicular Technology Conference: (VTC2022-Spring)*, Helsinki, Finland, 2022, pp. 1-6.

[28] X. Mu, Y. Liu, L. Guo, J. Lin and R. Schober, “Simultaneously Transmitting and Reflecting (STAR) RIS Aided Wireless Communications,” *IEEE Transactions on Wireless Communications*, vol. 21, no. 5, pp. 3083-3098, May 2022, doi: 10.1109/TWC.2021.3118225.

[29] X. Guan, Q. Wu and R. Zhang, “Intelligent Reflecting Surface Assisted Secrecy Communication: Is Artificial Noise Helpful or Not?,” *IEEE Wireless Communications Letters*, vol. 9, no. 6, pp. 778-782, June 2020.

[30] E. Basar and H. V. Poor, “Present and Future of Reconfigurable Intelligent Surface-Empowered Communications [Perspectives],” *IEEE Signal Processing Magazine*, vol. 38, no. 6, pp. 146-152, Nov. 2021, doi: 10.1109/MSP.2021.3106230.

[31] M. Makin, S. Arzykulov, K. M. Rabie and G. Nauryzbayev, “Performance Enhancement via Partitioning Large Intelligent Surfaces in Downlink NOMA Networks,” *2022 13th International Symposium on Communication Systems, Networks and Digital Signal Processing (CSNDSP)*, Porto, Portugal, 2022, pp. 379-383, doi: 10.1109/CSNDSP54353.2022.9907962.

[32] M. Makin, G. Nauryzbayev, S. Arzykulov and M. S. Hashmi, “Performance of Large Intelligent Surface-enabled Cooperative Networks Over Nakagami-m Channels,” *2021 IEEE 94th Vehicular Technology Conference (VTC2021-Fall)*, Norman, OK, USA, 2021, pp. 1-6, doi: 10.1109/VTC2021-Fall52928.2021.9625422.

[33] M. Makin, S. Arzykulov, A. Celik, A. M. Eltawil and G. Nauryzbayev, “Optimal RIS Partitioning and Power Control for Bidirectional NOMA Networks,” *IEEE Transactions on Wireless Communications*, doi: 10.1109/TWC.2023.3306048.

[34] P. Yang, L. Yang and S. Wang, “Performance Analysis for RIS-Aided Wireless Systems With Imperfect CSI,” *IEEE Wireless Communications Letters*, vol. 11, no. 3, pp. 588-592, March 2022, doi: 10.1109/LWC.2021.3136930.

[35] G. Zhou, C. Pan, H. Ren, K. Wang, M. D. Renzo and A. Nallanathan, “Robust Beamforming Design for Intelligent Reflecting Surface Aided MISO Communication Systems,” *IEEE Wireless Communications Letters*, vol. 9, no. 10, pp. 1658-1662, Oct. 2020, doi: 10.1109/LWC.2020.3000490.

[36] S. Hong, C. Pan, H. Ren, K. Wang, K. K. Chai and A. Nallanathan, "Robust Transmission Design for Intelligent Reflecting Surface-Aided Secure Communication Systems With Imperfect Cascaded CSI," *IEEE Transactions on Wireless Communications*, vol. 20, no. 4, pp. 2487-2501, April 2021, doi: 10.1109/TWC.2020.3042828.

[37] M. -M. Zhao, Q. Wu, M. -J. Zhao and R. Zhang, "Exploiting Amplitude Control in Intelligent Reflecting Surface Aided Wireless Communication With Imperfect CSI," *IEEE Transactions on Communications*, vol. 69, no. 6, pp. 4216-4231, June 2021, doi: 10.1109/TCOMM.2021.3064959.

[38] S. -Y. Jung, J. Hong and K. Nam, "Current Minimizing Torque Control of the IPMSM Using Ferrari's Method," *IEEE Transactions on Power Electronics*, vol. 28, no. 12, pp. 5603-5617, Dec. 2013, doi: 10.1109/TPEL.2013.2245920.

# Back Cover